Real-time chaotic video encryption based on multithreaded parallel confusion and diffusion

Dong Jiang[a,b,*], Zhen Yuan[a], Wen-xin Li[a], Liang-liang Lu[c,d,e,*]

[a]*School of Internet, Anhui University, Hefei, 230039, China*
[b]*National Engineering Research Center of Agro-Ecological Big Data Analysis and Application, Anhui University, Hefei, 230601, China*
[c]*Key Laboratory of Optoelectronic Technology of Jiangsu Province, Nanjing Normal University, Nanjing, 210023, China*
[d]*School of Physical Science and Technology, Nanjing Normal University, Nanjing, 210023, China*
[e]*National Laboratory of Solid State Microstructures, Nanjing University, Nanjing, 210093, China*

Abstract

Due to the strong correlation between adjacent pixels, most image encryption schemes perform multiple rounds of confusion and diffusion to protect the image against attacks. Such operations, however, are time-consuming, cannot meet the real-time requirements of video encryption. Existing works, therefore, realize video encryption by simplifying the encryption process or encrypting specific parts of video frames, which results in lower security compared to image encryption. To solve the problem, this paper proposes a real-time chaotic video encryption strategy based on multithreaded parallel confusion and diffusion. It takes a video as the input, splits the frame into subframes, creates a set of threads to simultaneously perform five rounds of confusion and diffusion operations on corresponding subframes, and efficiently outputs the encrypted frames. The encryption speed evaluation shows that our method significantly improves the confusion and diffusion speed, realizes real-time 480×480, 576×576, and 768×768 24FPS video encryption using Intel Core i5-1135G7, Intel Core i7-8700, and Intel Xeon Gold 6226R, respectively. The statistical and security analysis prove that the deployed cryptosystems have outstanding statistical properties, can resist attacks, channel noise, and data loss. Compared with previous works, to the best of our knowledge, the proposed strategy achieves the fastest encryption speed, and realizes the first real-time chaotic video encryption based on multi-round confusion-diffusion architecture, thus, providing a more secure and feasible solution for practical applications and related research.

Keywords: Real-time video encryption, Parallel computing, Chaotic systems, Confusion and diffusion

1. Introduction

With the rapid development of information and communication technologies, images and videos have shown enormous potential in data storage and network transmission, resulting in extensive application requirements for image and video encryption [1]. However, most conventional cryptographic schemes, such as DES, AES, RSA, etc., are designed to protect textual information, they are not suitable for images and videos [2]. As a result, many image encryption protocols have been proposed over recent years based on different techniques [3, 4, 5, 6], in which chaos based methods attract significant attention, due to the intrinsic characteristics of chaotic systems, including ergodicity, non-periodicity, non-convergence, sensitivity to initial conditions and control parameters, et al. [7]. Most chaos based image encryption algorithms comprises confusion and diffusion phases [8]. In the former phase, the pixel positions are scrambled over whole image without changing the values [9]. In the latter phase, the pixel values are modified sequentially with the byte sequences generated by chaotic systems [10].

Such confusion-diffusion architecture based image encryption protocols need to perform the two phases for multiple rounds until a satisfactory security level is achieved [11]. This, obviously, is very time-consuming and cannot meet the real-time requirements of video encryption. Existing works, therefore, realize video encryption through simplifying encryption process or encrypting specific pixels in the video[12, 13]. For the first category (also known as the full encryption), for example, Ref. [14] selects three chaotic maps to generate byte sequences, and directly performs XOR operations between the pixels and the generated bytes to encrypt the video; Refs. [15] use the generated bytes to encrypt the frame, and take the encrypted pixels as feedback to improve the plaintext sensitivity of the deployed cryptosystem; Ref. [16] performs one round of confusion operation on the video frame, followed by acting XOR operations between the pixels and the generated bytes to realize frame encryption; Since practical applications put forward higher requirements for security, most recently published works are based on one-round confusion-diffusion architecture[17, 18, 19, 20, 21, 22]. The second category is also known as the selective encryption, the algorithms belong to this category encrypt specific pixels in the video frame to reduce the computational complexity [23]. These categories of strategies, clearly, achieve high efficiency at the expense of security.

---

*Corresponding author.
    Email addresses:* `jiangd@nju.edu.cn` (Dong Jiang),
`liangliianglu@nju.edu.cn` (Liang-liang Lu)

Therefore, how to realize real-time video encryption without compromising the security has become an urgent problem to be solved. In the field of full video encryption, however, there are few related research. And to the best of our knowledge, existing works cannot realize real-time video encryption, i.e., the the number of frames encrypted in a second is larger than FPS (Frames Per Second) of the video or the average encryption time (ms) is less than 1000 / FPS. This paper, thus, takes the advantage of parallel computing, designs a five-round confusion-diffusion architecture based real-time chaotic video encryption strategy. To evaluate the performance, two cryptosystems are implemented using two different chaotic maps. Three hardware platforms are used to assess the encryption speed of the deployed cryptosystems. The evaluation results show that our strategy significantly improves the speed of byte generation, confusion, and diffusion, laying the foundation for the realization of real-time video encryption. The statistical and security analysis prove that the deployed cryptosystems have outstanding statistical properties and resistance to attacks, channel noise and data loss. The proposed strategy also suitable for many confusion and diffusion methods, and can be easily realized with both software and hardware.

The rest of the paper are organized as follows: section 2 gives a detailed description of the proposed strategy. In section 3, two typical chaotic maps are selected to realize the strategy, and the encryption speed of the deployed cryptosystems are evaluated using three different hardware platforms. Section 4 and 5 carry out statistical and security analysis, respectively. Section 6 analyzes the reasons for the parameter settings used in this paper. In section 7 gives a comparison to recent published works, followed by a brief conclusion in section 8.

2. Strategy Description

In the proposed strategy, as shown in Fig. 1, a set of threads are used to encrypt the video frames, simultaneously. These threads can be divided into two categories: a main thread T_m and n assistant threads T_a^i ($i \in \{0, ..., n-1\}$). The main thread takes the key K and the original video V as input, initializes its $PRBG_m$, generates the parameters P_m, creates and organizes T_as to perform confusion and diffusion operations on the video frames. See Algo. 1 for the detailed encryption process of T_m.

Algorithm 1: Encryption process of main thread T_m.

Input: Key: K; Number of assistant threads: n; Video file: V; Rounds of confusion and diffusion operations: r.

Output: Parameters for initializing $PRBG_a$s of T_as: P_m; Plain Frame: F_p; Confusion seed: s_c.

Initialize $PRBG_m$ with K;
Iterate $PRBG_m$, generate enough iteration results;
Convert iteration results to parameters P_m;
for $i = 0; i < n; i++$ **do**
  Create the assistant thread T_a^i;

while Fetch a frame F_p from V **do**
  Iterate $PRBG_m$, and generate a confusion seed s_c;
  for $i = 0; i < r; i++$ **do**
    Awake T_as to perform confusion operation;
    Wait for T_as to finish the confusion operation;
    Awake T_as to perform diffusion operation;
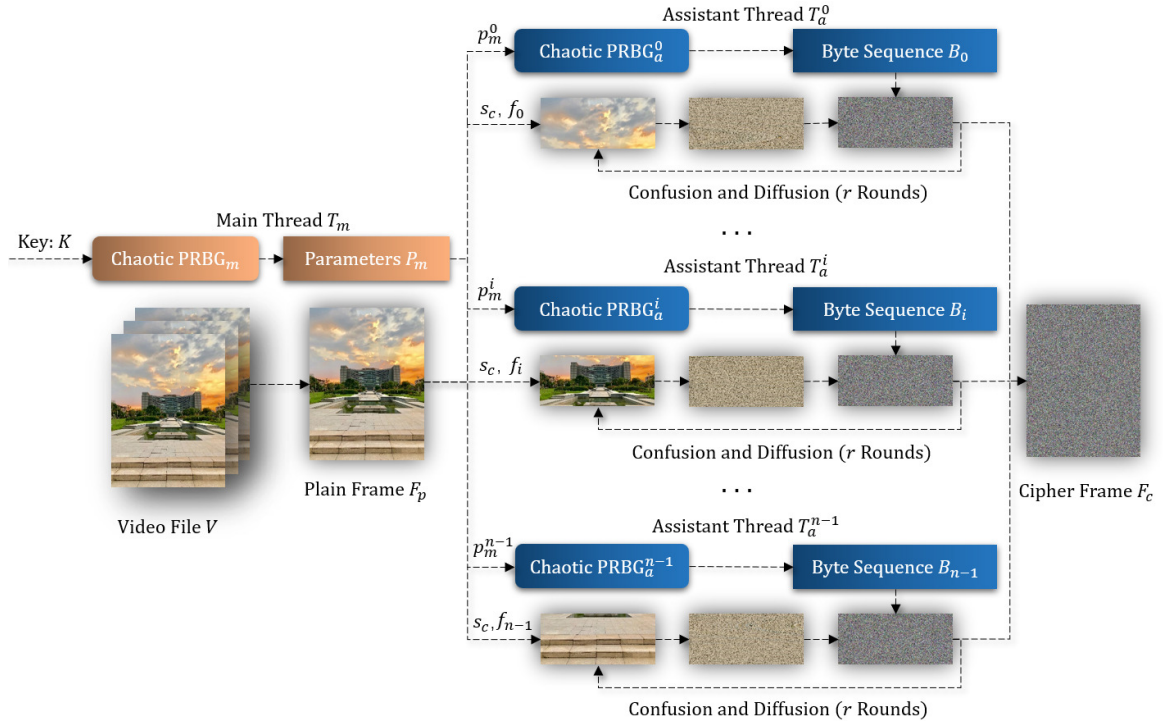   Wait for T_as to finish the diffusion operation;

Figure 1: Workflow diagram of the proposed chaotic real-time video encryption strategy (p_m: parameters generated by $PRBG_m$; s_c: confusion seed; f: subframe).

Assistant thread T_a^i, initializes its $PRBG_a^i$ with parameters $p_m^i \in P_m$, generates iteration results, converts the results into byte sequence B_i, performs confusion and diffusion operations on the subframe f_i, and outputs the cipher frame F_c. In confusion operation, a discretized version of the Chirikov normal map [24] as follows is used to rearrange the pixel positions:

$$\begin{cases} \alpha = (a + o) \bmod w, \\ \beta = (o + s_c \sin(2\pi\alpha/w)) \bmod w, \end{cases} \quad (1)$$

where a and o are the abscissa and ordinate of the pixel, α and β are the new coordinates of the pixel after confusion operation, w is the width of the video frame, and s_c is referred to as the confusion seed, which is a positive integer generated by T_m. The inverse transform of confusion operation is as follows:

$$\begin{cases} a = (\alpha - \beta + s_c \sin(2\pi\alpha/w)) \bmod w, \\ o = (\beta - s_c \sin(2\pi\alpha/w)) \bmod w. \end{cases} \quad (2)$$

Algorithm 2: Encryption process of assistant thread T_a^i.

Input: Thread index: i; Number of assistant threads: n;
      Plain frame: F_p; Width of F_p: w; Parameters
      generated by T_m: P_m; Rounds of confusion and
      diffusion r; Confusion seed: s_c.

Output: Cipher frame: F_c.

startRow $= i \times w/n$;
endRow $=$ startRow $+w/n$;
Initialize $PRBG_a^i$ with p_m^i;
while Fetch subframe f_i from F_p **do**
  Iterate $PRBG_a^i$, generate enough iteration results;
  Convert iteration results into byte sequence B_i;
  $F_c = F_p$;
  for $j = 0; j < r; j + +$ **do**
    Wait to be woken up by T_m;
    Temp frame $F_t = F_c$;
    for $a =$ startRow; $a <$ endRow; $a + +$ **do**
      for $o = 0; o < w; o + +$ **do**
        $\alpha = (a + o) \bmod w$;
        $\beta = (o + s_c \sin(2\pi\alpha/w)) \bmod w$;
        $F_c[\alpha,\beta] = F_t[a,o]$;
    Tell T_m that the confusion operation is completed
    Wait to be woken up by T_m
    $F_t = F_c$;
    Take the last pixel of $f_{(i+1)\bmod n}$ as diffusion seed
     s_d;
    for $a =$ startRow; $a <$ endRow; $a + +$ **do**
      for $o = 0; o < w; o + +$ **do**
        Fetch a byte b from B_i;
        if $a ==$ startRow AND $o == 0$ **then**
          $F_c[a,o] = b \oplus (F_t[a,o] + b) \oplus s_d$;
        else
          Fetch previous pixel $F_c[a',o']$;
          $F_c[a,o] = b \oplus (F_t[a,o]+b) \oplus F_c[a',o']$;
    Tell T_m that the diffusion operation is completed

In diffusion, the following equation is employed[25]:

$$F_c[a, o] = b \oplus (F_p[a, o] + b) \oplus F_c[a', o'], \quad (3)$$

where $F_c[a, o]$ and $F_p[a, o]$ denote the encrypted and the plain pixel, b is a byte generated by $PRBG_a^i$, and $[a', o']$ is the coordinate of previous pixel. To perform diffusion operation, the diffusion seed s_d needs to be set to encrypt $F_p[0, 0]$. In the proposed strategy, T_a^i takes the last pixel of subframe $f_{(i+1)\bmod n}$ as s_d. The inverse transform of diffusion is as follows:

$$F_p[a, o] = (b \oplus F_c[a, o] \oplus F_c[a', o']) - b. \quad (4)$$

See Algo. 2 for the detailed encryption process of T_a^i.

3. Encryption Speed Evaluation

To evaluate the encryption speed of the proposed strategy, two highly-cited chaotic maps are selected to implement PRBGs. The first PRBG uses two Piecewise Linear Chaotic Maps (PLCM) [26], which is defined as follows:

$$x_{i+1} = F(x_i, p) = \begin{cases} x_i/p, & x_i \in [0, p) \\ (x_i - p)/(\frac{1}{2} - p), & x_i \in [p, 0.5], \\ F(1 - x_i, p), & x_i \in (0.5, 1] \end{cases} \quad (5)$$

where $x_i \in [0, 1]$, x_0 and $p \in (0, 0.5)$ are referred to as the initial condition and the control parameter, respectively. The second PRBG employs couple two dimensional Logistic-Adjusted-Sine Map (2DLASM) [27], which is given by:

$$\begin{cases} x_{i+1} = \sin(\pi\mu(y_i + 3)x_i(1 - x_i)), \\ y_{i+1} = \sin(\pi\mu(x_{i+1} + 3)y_i(1 - y_i)), \end{cases} \quad (6)$$

where $x_i, y_i \in [0, 1]$, x_0 and $\mu \in [0.37, 0.38] \cup [0.4, 0.42] \cup [0.44, 0.93] \cup \{1\}$ are referred to as the initial condition and the control parameter, respectively.

Three hardware platforms are selected to carry out the evaluations. The specifications of the platforms are listed in Tab. 1. The software development environment are as follows: Ubuntu 20.04 operating system, OpenCV 4.2.0, and g++ 9.4.0.

Table 1: The specifications of hardware platforms

Platform	Specifications	
Laptop	CPU	Intel Core i5-1135G7
	Cores / Threads	4 / 8
	Frequency	2.4GHz
	Memory	8GB
Personal Computer	CPU	Intel Core i7-8700
	Cores / Threads	6 / 12
	Frequency	3.2GHz
	Memory	32GB
Workstation	CPU	Intel Xeon Gold 6226R
	Cores / Threads	16 / 32
	Frequency	2.9GHz
	Memory	64GB

Since the encryption process of the proposed strategy consists of byte generation, confusion, and diffusion, we implement two cryptosystems using the selected chaotic maps, separately evaluate the speed of these steps, and assess the video encryption speed of the deployed cryptosystesm. In these experiments, the keys K used to initialize $PRBG_m$ are randomly selected, the original video is downloaded from the video trace library, and is converted into different sizes for encryption speed evaluation.

First, different number of assistant threads are used to generate byte sequences, simultaneously. In PLCM based cryptosystem, the assistant thread T_a^i uses p_m^i generated by the main thread T_m to initialize its $PRBG_a^i$, iterates PLCMs and generates two sets of iteration results $\{x_1^1, x_2^1, x_3^1...\}$, $\{x_1^2, x_2^2, x_3^2...\}$, fetches 6 bytes from the mantissa part[1] of each iteration result, and produces two sets of byte sequences $\{b_1^1, b_2^1, b_3^1, ...\}$, $\{b_1^2, b_2^2, b_3^2, ...\}$. By sequentially performing XOR operations on the generated bytes, T_a^i outputs the final byte sequence B_i, which can be used for video encryption and decryption. In 2DLASM based cryptosystem, similarly, T_a^i uses p_m^i to initialize its $PRBG_a^i$, iterates the 2DLASMs and generates two sets of iteration results $\{x_1^1, y_1^1, x_2^1, y_2^1, ...\}$, $\{x_1^2, y_1^2, x_2^2, y_2^2, ...\}$. By fetching 6 bytes from each iterations result and acting XOR operations on the generated bytes, T_a^i produces the byte sequence B_i. To calculate the throughput, all chaotic maps are iterated for 5×10^7 times. The relationship between the throughput (MBps) and the number of assistant threads are shown in Fig. 2 (a)-(c).

---

[1] In IEEE 754 standard, a double precision floating-point number consists of 1 bit sign, 11 bits exponent, and 52 bits mantissa fields.

Second, we set the rounds of confusion and diffusion r to 5 (see section 6 for the reasons), perform five rounds of confusion operations on 100 images of size 960×960 with different number of assistant threads, calculate the average time to scramble an image, and plot the results in 2 (d)-(f). Similarly, we use different number of assistant threads to generate byte sequences, perform five rounds of diffusion operations on 100 images of size 960×960 using the generated bytes, and calculate the average time to complete five rounds of diffusion operations on an image. The relationship between the average diffusion time (including byte generations and diffusion operations) are drawn in Fig. 2 (g)-(i). Compared with the single-threaded versions of byte generation, confusion, and diffusion, clearly, the proposed strategy significantly speeds up these steps.

Third, to evaluate the practical performance of the proposed strategy, a set of videos of different sizes are encrypted using the deployed cryptosystems. Similar to above experiments, the rounds of confusion and diffusion r is set to 5. The number of assistant threads n are set to 8, 12, and 32 for laptop, personal computer, and workstation, respectively (see section 6 for the reasons). The Frames Per Second (FPS) of the selected vidoes is 20, that is, the maximum time for encrypting a frame must be less than 50ms, otherwise, there will exist delay during encryption and transmission. Each video consists of 600 frames. The average encryption time are listed in Tab. 2, which shows that real-time 576×576, 672×672, and 960×960 video encryption are realized using Intel Core i5-1135G7, Intel Core i7-8700, and Intel Xeon Gold 6226R, respectively.
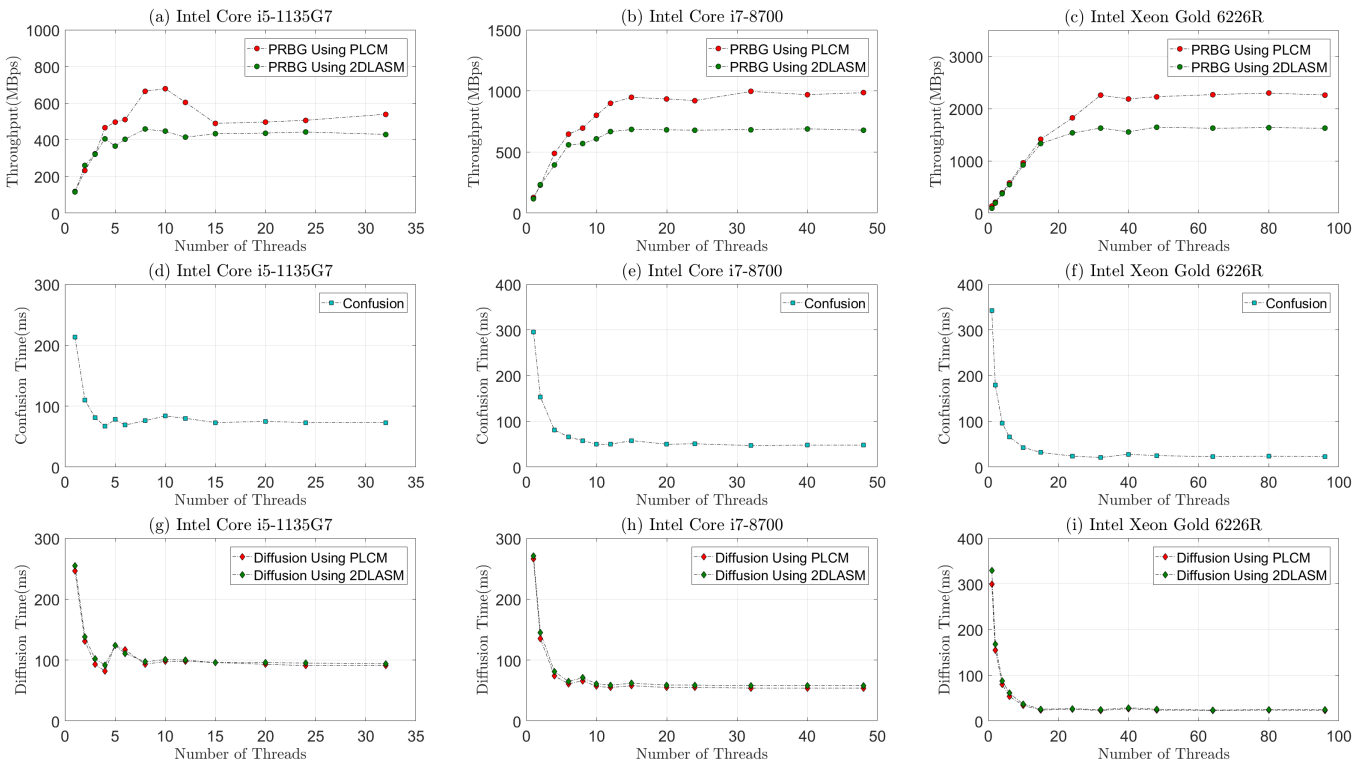

Figure 2: Speed evaluation of byte generation, confusion, and diffusion steps, (a-c) throughput of all $PRBG_a$s versus the number of assistant threads, (d-f) average time of confusion operations versus the number of assistant threads, (g-i) average time of diffusion operations versus the number of assistant threads.

4

Table 2: Video encryption speed evaluation.

Video Size	Max Encryption Time	Laptop (8 T_as) Average Encryption Time(ms)		Personal Computer (12 T_as) Average Encryption Time(ms)		Workstation (32 T_as) Average Encryption Time(ms)	
		PLCM	2DLASM	PLCM	2DLASM	PLCM	2DLASM
96×96	42ms	5.69	5.54	7.43	7.40	2.92	2.62
192×192	42ms	16.59	16.56	21.45	20.92	7.69	7.41
288×288	42ms	29.63	28.98	30.39	31.76	15.12	14.94
384×384	42ms	31.60	30.64	35.97	35.22	23.25	22.94
480×480	42ms	36.26	35.49	37.76	37.88	28.76	28.11
576×576	42ms	$\times$	$\times$	39.92	40.67	30.40	30.02
672×672	42ms	$\times$	$\times$	$\times$	$\times$	33.60	32.89
768×768	42ms	$\times$	$\times$	$\times$	$\times$	36.56	36.23

Number of Frames: 300; FPS: 24; Rounds of confusion and diffusion: $r = 5$; $\times$: Average Encryption Time $\geq$ Max Encryption Time.

4. Statistical Evaluation

The essence of real-time video encryption is image encryption, which should provide excellent statistical properties to resist different types of attacks [28]. In this section, therefore, the uniformity, correlation, and randomness of the deployed cryptosystems are analyzed. The following experiments are performed using the laptop (Intel Core i5-1135G7), and the parameter setup are as follows: number of assistant threads: $n = 8$, confusion and diffusion rounds $r = 5$, the size of all plain images used for statistical evaluation is 512×512.

4.1. Uniformity Evaluation

The histogram, variances and χ^2 of histograms are utilized to evaluate the uniformity of the deployed cryptosystems. The plain image is plotted in Fig. 3 (a), and its histograms of red, green, blue channels are shown in 3 (b), (c), (d), respectively. The cipher image encrypted with PLCM is shown in Fig. 3 (e). Its histograms of red, green, blue channels are shown in Fig. 3 (f), (g), (h), respectively. The cipher image encrypted with 2DLASM is shown in Fig. 3 (f). Its histograms of red, green, blue channels are shown in Fig. 3 (j), (k), (l), respectively.

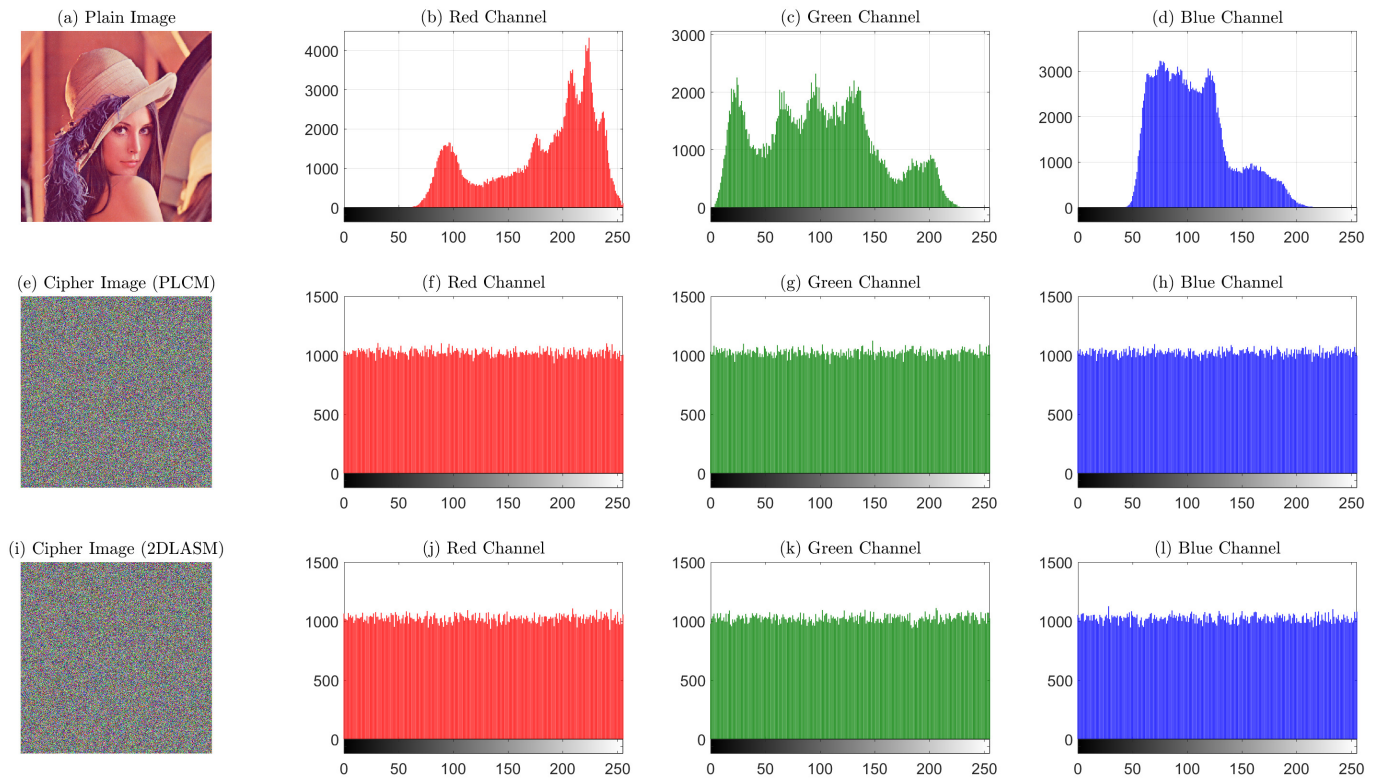Figure 3: Histograms of plain and cipher images. (a) plain image Lena, (b) - (d) histograms of the red, green, and blue channels of the plain image, (e) cipher image encrypted with PLCM, (f) - (h) histograms of the red, green, and blue channels of the cipher image encrypted with PLCM, (i) cipher image encrypted with 2DLASM, (h) - (j) histograms of the red, green, and blue channels of the cipher image encrypted with 2DLASM.

The variance of an image can be calculated as follows [29]:

$$\text{var(Z)} = \frac{1}{256^2} \sum_{i=0}^{255} \sum_{j=0}^{255} \frac{1}{2}(z_i - z_j)^2, \tag{7}$$

where $Z = \{z_0, z_1, ..., z_{255}\}$ is the vector of the histogram values, z_i and z_j are the numbers of pixels whose values are equal to i and j, respectively. The χ^2 of an image is given by [30]:

$$\chi^2 = \sum_{i=0}^{255} \frac{(z_i - N/256)^2}{N/256}, \tag{8}$$

where N is the number of pixels, $N/256$ is the expected occurrence frequency. The higher variance indicates the lower uniformity of an image, and when the significant level is 0.05, $\chi^2(0.05, 255)$ is equal to 293.25 [31]. We encrypt a set of images using PLCM and 2DLASM, respectively, calculate and list the variance and χ^2 test results of plain and cipher images in Tab. 3. Clearly, the variances of the cipher images are significantly reduced compared to the variances of the corresponding plain images, and χ^2 values of the cipher images are lower than 293.25. The deployed cryptosystems, therefore, uniformly conceal the information of the plain images.

4.2. Correlation Evaluation

Since two adjacent pixels in an image usually have high correlation, the cryptosystems should decrease the correlation to resist statistical attacks [32]. Therefore, the correlation between two adjacent pixels in plain and cipher images are analyzed. We first randomly select 6000 pairs of two horizontally, vertically, and diagonally adjacent pixels from the plain and cipher images. The correlation distribution of red, green, and blue channels in plain image shown in Fig. 4 (a), (b), (c), respectively. The correlation distribution of red, green, and blue channels in cipher image are plotted in Fig. 4 (d), (e), (f), respectively. The correlation distribution of red, green, and blue channels in cipher image shown in Fig. 3 (i) are drawn in Fig. 4 (g), (h), (i), respectively.

Then, the correlation coefficient between adjacent pixels are measured. The correlation coefficient $r_{x,y}$ of adjacent pixels can be calculated out according to the following equation [33]:

$$r_{x,y} = \frac{\text{cov}(x, y)}{\sqrt{D(x)D(y)}}, \tag{9}$$

where x and y are the values of two adjacent pixels in the image, $\text{cov}(x, y)$ is given by

$$\text{cov}(x, y) = \frac{1}{N} \sum_{i=1}^{N} (x_i - E(x))(y_i - E(y)), \tag{10}$$

N is the total number of pixels selected from the image for the calculation, $E(x)$ and $D(x)$ are defined as follows:

$$E(x) = \frac{1}{N} \sum_{i=1}^{N} x_i, \tag{11}$$

$$D(x) = \frac{1}{N} \sum_{i=1}^{N} (x_i - E(x))^2. \tag{12}$$

When the correlation coefficient of a cipher image is lower, the resistance capability of the encryption algorithm to statistical analysis attacks is stronger. To assess the correlation property of the proposed strategy, we encrypt a set of plain images using PLCM and 2DLASM, randomly select 20000 adjacent pixels in horizontal, vertical, and diagonal directions from the plain and cipher images, calculate the correlation coefficients, and list the results in Tab. 4. The deployed cryptosystesm, clearly, significantly decrease the correlation of the plain images.

Table 3: Variances and χ^2 results of plain and cipher images

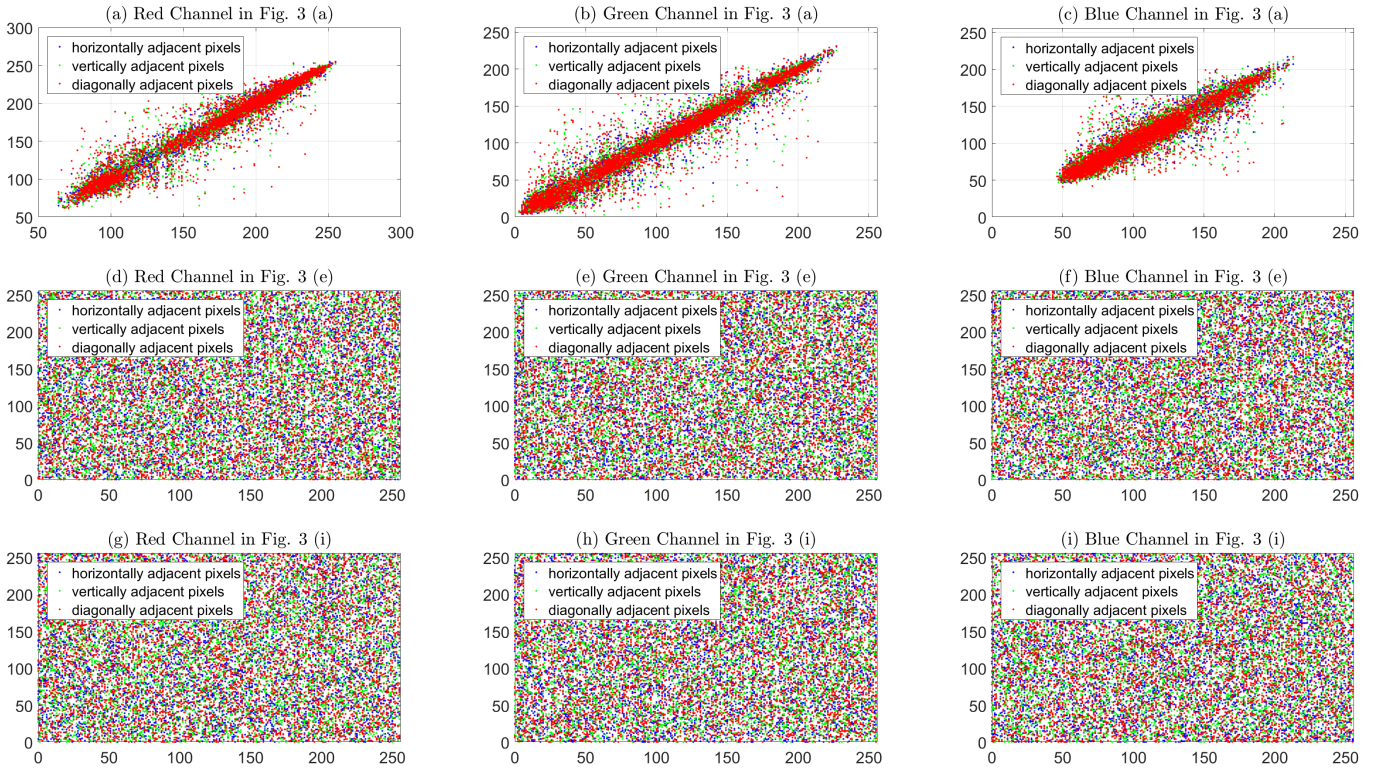| Test	Image	Channel		
		R	G	B
var	Lena	1021324	457505	1382757
	Lena (PLCM)	920.81	982.86	802.76
	Lena (2DLASM)	1078.06	1047.92	1065.47
	Airplane	2724339	2740687	4448810
	Airplane (PLCM)	1139.74	1043.63	930.89
	Airplane (2DLASM)	1022.57	1115.45	1035.92
	Lake	789874	522660	1383691
	Lake (PLCM)	942.18	1019.14	1166.58
	Lake (2DLASM)	1063.56	913.51	1068.22
	Peppers	856092	1278525	1973421
	Peppers (PLCM)	981.84	995.96	919.01
	Peppers (2DLASM)	1030.07	946.35	1101.70
	Mandrill	332658	573472	321024
	Mandrill (PLCM)	1018.60	1016.43	1138.86
	Mandrill (2DLASM)	1165.99	993.28	872.41
	Splash	2432151	3095990	5940168
	Splash (PLCM)	1015.49	1112.96	1072.76
	Splash (2DLASM)	954.40	880.06	1127.92
χ^2	Lena	254333	113929	344338
	Lena (PLCM)	229.30	244.75	199.90
	Lena (2DLASM)	268.46	260.95	265.32
	Airplane	678424	682495	1107858
	Airplane (PLCM)	283.82	259.88	231.81
	Airplane (2DLASM)	254.64	277.77	257.96
	Lake	196697	130154	344571
	Lake (PLCM)	234.62	253.79	290.50
	Lake (2DLASM)	264.85	227.48	266.01
	Peppers	213187	318382	491428
	Peppers (PLCM)	244.50	248.01	228.85
	Peppers (2DLASM)	256.51	235.66	274.34
	Mandrill	82839	142808	79942
	Mandrill (PLCM)	253.65	253.11	283.60
	Mandrill (2DLASM)	290.35	247.35	217.25
	Splash	605662	770974	1479241
	Splash (PLCM)	252.88	277.15	267.14
	Spalsh (2DLASM)	237.66	219.15	280.88

Figure 4: Correlation distribution of two adjacent pixels in horizontal, vertical, and diagonal directions, (a) - (c) correlation distribution of red, green, and blue channels in plain image, (d) - (f) correlation distribution of red, green, and blue channels in cipher image encrypted with PLCM, (g) - (i) correlation distribution of red, green, and blue channels in cipher image encrypted with 2DLASM.

Table 4: Correlation coefficients of two adjacent pixels in the plain and cipher images

Image	Channel	Plain Image			Cipher Image Encrypted With PLCM			Cipher Image Encrypted With 2DLASM		
		H	V	D	H	V	D	H	V	D
Lena	R	0.988469	0.980273	0.968900	-0.003864	- 0.000723	-0.009886	-0.001331	-0.003863	-0.002300
	G	0.980549	0.968197	0.951883	0.013827	0.003009	0.002088	-0.008544	-0.002600	-0.012616
	B	0.951984	0.927028	0.908143	0.003075	0.002843	0.003700	-0.002474	0.001525	-0.016043
Airplane	R	0.970642	0.970695	0.945469	0.006467	-0.006111	0.003168	0.001575	0.011213	-0.008233
	G	0.971925	0.926737	0.902899	-0.004944	0.003830	-0.017420	-0.003714	0.001359	-0.008748
	B	0.956298	0.959205	0.930419	-0.001179	-0.000550	-0.002195	-0.001821	-0.000839	0.003026
Lake	R	0.954300	0.950933	0.938652	-0.002712	-0.002231	-0.007473	0.008294	0.002791	0.005007
	G	0.968942	0.972935	0.957351	-0.006042	0.005319	-0.003452	-0.005502	-0.003010	-0.000647
	B	0.968070	0.969546	0.951428	0.005635	-0.003997	0.002186	0.010300	-0.003263	0.001231
Peppers	R	0.968357	0.956775	0.950391	-0.000807	-0.004586	-0.001847	-0.002638	0.007745	0.005794
	G	0.986690	0.972400	0.964351	0.004994	0.011397	0.008190	0.003480	0.004427	0.004097
	B	0.972810	0.959227	0.947239	-0.003806	0.007530	-0.006979	-0.003785	-0.004886	-0.001596
Mandrill	R	0.853960	0.910030	0.841495	0.000305	-0.009033	0.004641	0.010308	0.004073	0.007677
	G	0.771212	0.858922	0.739454	0.000354	0.006221	-0.000766	-0.008846	-0.006407	0.000659
	B	0.864290	0.892019	0.825914	0.005260	-0.007633	0.001064	0.002351	-0.010925	0.009007
Splash	R	0.985901	0.992967	0.980009	0.012251	-0.003002	-0.005989	-0.002299	0.005270	0.005558
	G	0.979680	0.981868	0.965632	0.006494	0.003150	-0.006994	0.001839	-0.002984	0.001348
	B	0.959442	0.983775	0.948882	0.015445	0.003662	-0.009827	-0.006020	-0.010502	0.002206

H: horizontal correlation coefficient; V: vertical correlation coefficient; D: diagonal correlation coefficient.

4.3. Randomness Evaluation

In this section, three widely used methods, i.e., information entropy, (k, T_B) local Shannon entropy, and NIST statistical tests, are employed to evaluate the randomness properties of the proposed strategy. The information entropy is defined to quantify the information randomness [34]. For a given information m, the entropy $H(m)$ can be calculated as follows:

$$H(m) = \sum_{i=1}^{N} p(m_i) \log \frac{1}{p(m_i)}, \qquad (13)$$

where N is the total number of symbols, and $p(m_i)$ is the occurrence probability of symbol m_i. For a random figure F, the entropy $H(F)$ equals to 8. A cryptosystem, therefore, should generate cipher image with information entropy close to 8.

The (k, T_B) local Shannon entropy is utilized to measure the local randomness of images [35], it is defined as follows:

$$\overline{H}_{k,T_B} = \sum_{i=1}^{k} \frac{H(M_i)}{k}, \qquad (14)$$

where M_i ($i \in \{1, 2, ..., k\}$) are the randomly selected non-overlapping image sub-blocks, each block has T_B pixels, $H(M_i)$ is the information entropy of block M_i. We encrypt a set of plain images with randomly selected key K using PLCM and 2DLASM, respectively, list the information entropy results in Tab. 5. Then we set k and T_B to 30 and 1936 according to Refs. [36, 37], randomly select non-overlapping blocks from the plain and the generated cipher images, calculate $\overline{H}_{k,T_B}$. and list the results in Tab. 5.

NIST statistical test suite (version 800-22) can be used to test if a sequence generated by random or pseudorandom number generators is suitable for cryptographic applications [38]. It consists fifteen statistical tests focusing on distinct types of nonrandomness that may exist in a bit sequence. The tests are used to determine the acceptance of the hypothesis of ideal randomness with significance level α, which is set to 0.01. For each test, P-value and pass rate r_p are regarded as the criteria results. When P-value is larger than the significance level α, the sequence is regard as random. In video encryption, the assistant threads take a subframe, generate byte sequence, and perform diffusion operation on the subframe. According to the encryption process, we use 8 assistant threads T_a^i $i \in \{1, 2, ..., 8\}$ to generate enough byte sequences $B_1, B_2, ..., B_8$ using PLCM and 2DLASM, respectively. And perform NIST tests on the generated bytes. The results are shown in Tab. 6.

Table 5: Information entropy H and (k, T_B)-local Shannon entropy $\overline{H}_{k,T_B}$ of plain and cipher images.

Test	Image	Channel		
		R	G	B
H	Lena	7.253102	7.594038	6.968427
	Lena (PLCM)	7.999369	7.999326	7.999449
	Lena (2DLASM)	7.999259	7.999282	7.999269
	Airplane	6.717765	6.798979	6.213774
	Airplane (PLCM)	7.999219	7.999286	7.999361
	Airplane (2DLASM)	7.999299	7.999234	7.999291
	Lake	7.312388	7.642854	7.213642
	Lake (PLCM)	7.999353	7.999302	7.999199
	Lake (2DLASM)	7.999271	7.999373	7.999268
	Peppers	7.338827	7.496253	7.058306
	Peppers (PLCM)	7.999328	7.999317	7.999370
	Peppers (2DLASM)	7.999292	7.999353	7.999245
	Mandrill	7.706672	7.474432	7.752217
	Mandrill (PLCM)	7.999302	7.999302	7.999221
	Mandrill (2DLASM)	7.999201	7.999319	7.999403
	Splash	6.948061	6.884455	6.126452
	Splash (PLCM)	7.999305	7.999238	7.999263
	Splash (2DLASM)	7.999346	7.999397	7.999225
$\overline{H}_{k,T_B}$	Lena	5.911418	6.378169	6.044504
	Lena (PLCM)	7.901188	7.900454	7.902854
	Lena (2DLASM)	7.903580	7.902076	7.901568
	Airplane	5.371063	5.348903	4.918050
	Airplane (PLCM)	7.903643	7.901751	7.902929
	Airplane (2DLASM)	7.903149	7.904907	7.901914
	Lake	6.129053	6.348979	5.847770
	Lake (PLCM)	7.906276	7.901353	7.901770
	Lake (2DLASM)	7.902562	7.900261	7.901848
	Peppers	5.975824	6.057454	5.870517
	Peppers (PLCM)	7.903389	7.905916	7.901726
	Peppers (2DLASM)	7.902408	7.899511	7.904691
	Mandrill	6.578668	6.688874	6.802597
	Mandrill (PLCM)	7.903176	7.901764	7.903579
	Mandrill (2DLASM)	7.901823	7.901584	7.903498
	Splash	4.150002	5.184026	4.560897
	Splash (PLCM)	7.903036	7.902193	7.903928
	Spalsh (2DLASM)	7.900637	7.904737	7.902950

Table 6: Results of NIST tests.

Statistical Test	PLCM		2DLASM	
	P-value	$r_p(\%)$	P-value	$r_p(\%)$
Frequency	0.181557	99	0.657933	98
Block Frequency	0.474986	99	0.955835	99
Cumulative Sums*	0.452541	99	0.717629	98
Runs	0.350485	99	0.115387	97
Longest Run	0.883171	97	0.171867	100
Rank	0.366918	99	0.554420	100
FFT	0.897763	100	0.595549	100
Non Overlapping Template*	0.486724	99	0.510463	98
Overlapping Template	0.366918	98	0.883171	96
Universal	0.455937	100	0.574903	97
Approximate Entropy	0.983453	99	0.249284	98
Random Excursions*	0.415715	99	0.258140	99
Random Excursions Variant*	0.442424	99	0.276585	99
Serial*	0.428515	99	0.944186	99
Linear Complexity	0.137282	96	0.058984	100

Significance level $\alpha = 0.01$; r_p: pass rate; *: mean value.

5. Security Analysis

5.1. Key Space And Sensitivity

One of the most important issue of the security of cryptosystems is the key. According to the Kerckhoff's principle, a cryptosystem should be secure even though everything about the system, except the key, is known by the cracker [39]. If the key is poorly chosen or the key space is too small, no matter how strong the encryption algorithm might be, the cryptosystem can be easily cracked. It is generally accepted that the key space of a cryptosystem should be large that 2^{100} to provide a sufficient security against ciphertext only attaks [40]. For the proposed strategy, clearly, the key is the parameters that used to initialize $PRBG_m$ of the main thread T_m. In PLCM based cryptosystesm, four double precision floating-point numbers are taken as the initial conditions and control parameters to initialize two PLCMs. In the 2DLASM based cryptosystem, three double precision floating-point numbers are input as the initial condition x_0, control parameter μ, and y_0 to initialize 2DLASM. The key space of PLCM and 2DLASM based cryptosystems, therefore, are 2^{256} and 2^{192}, respectively. This clearly, provides the resistance to ciphertext only attacks. The users can employ more complex PRBG to obtain larger key space, resulting in higher security.

In addition, the cryptosystem should have high sensitivity to the change of key in encryption and decryption process. That is, even one bit of the key is changed, the attacker cannot obtain any information from the decrypted image. To analyze the key sensitivity of the proposed strategy, we randomly select key, use the deployed cryptosystems to ecnrypt an iamge, followed by decrypting the cipher image with the correct key. The images decrypted with PLCM and 2DLASM are plotted in Fig. 5 (a) and (e), respectively. Then we slight change the key by adding an increment $\delta = 0.000000001$ on initial condition and control parameter, decrypted the cipher image with the slightly modified Key. The images decrypted by PLCM based cryptosystem using $x_0 + \delta$, $p + \delta$, and $x_0 + \delta, p + \delta$ are shown in Fig. 5 (b), (c), and (d), respectively. The images decrypted by 2DLASM based cryptosystem using $x_0 + \delta$, $\mu + \delta$, and $x_0 + \delta, \mu + \delta$ are shown in Fig. 5 (f), (g), and (h), respectively. We also calculate the correlation coefficients between the images decrypted with the correct key and the images decrypted with the slightly changed key, and list the results in Tab. 7.

Table 7: Correlation coefficients between decrypted images plotted in Fig. 5.

PRBG	Images	Channel		
		R	G	B
PLCM	Fig. 5 (a), (b)	-0.002588	0.005312	0.002903
	Fig. 5 (a), (c)	-0.001788	0.001664	-0.001074
	Fig. 5 (a), (d)	-0.002994	0.001132	0.002672
	Fig. 5 (b), (c)	0.004292	-0.001097	-0.000042
	Fig. 5 (b), (d)	0.002267	0.001098	0.002168
	Fig. 5 (c), (d)	0.000715	0.004356	0.000954
2DLASM	Fig. 5 (e), (f)	-0.002142	0.000862	0.000712
	Fig. 5 (e), (g)	-0.002620	0.001053	-0.000951
	Fig. 5 (e), (h)	0.003072	-0.000513	0.001539
	Fig. 5 (f), (g)	-0.001342	-0.000709	0.002444
	Fig. 5 (f), (h)	0.004969	-0.001565	0.000370
	Fig. 5 (g), (h)	0.003579	0.001962	0.000740

(a) Decrypted image with correct key (PLCM) (b) Decrypted image with $x_0 + \delta$ (PLCM) (c) Decrypted image with $p + \delta$ (PLCM) (d) Decrypted image with $x_0 + \delta, p + \delta$ (PLCM)

(e) Decrypted image with correct key (2DLASM) (f) Decrypted image with $x_0 + \delta$ (2DLASM) (g) Decrypted image with $\mu + \delta$ (2DLASM) (h) Decrypted image with $x_0 + \delta, \mu + \delta$ (2DLASM)
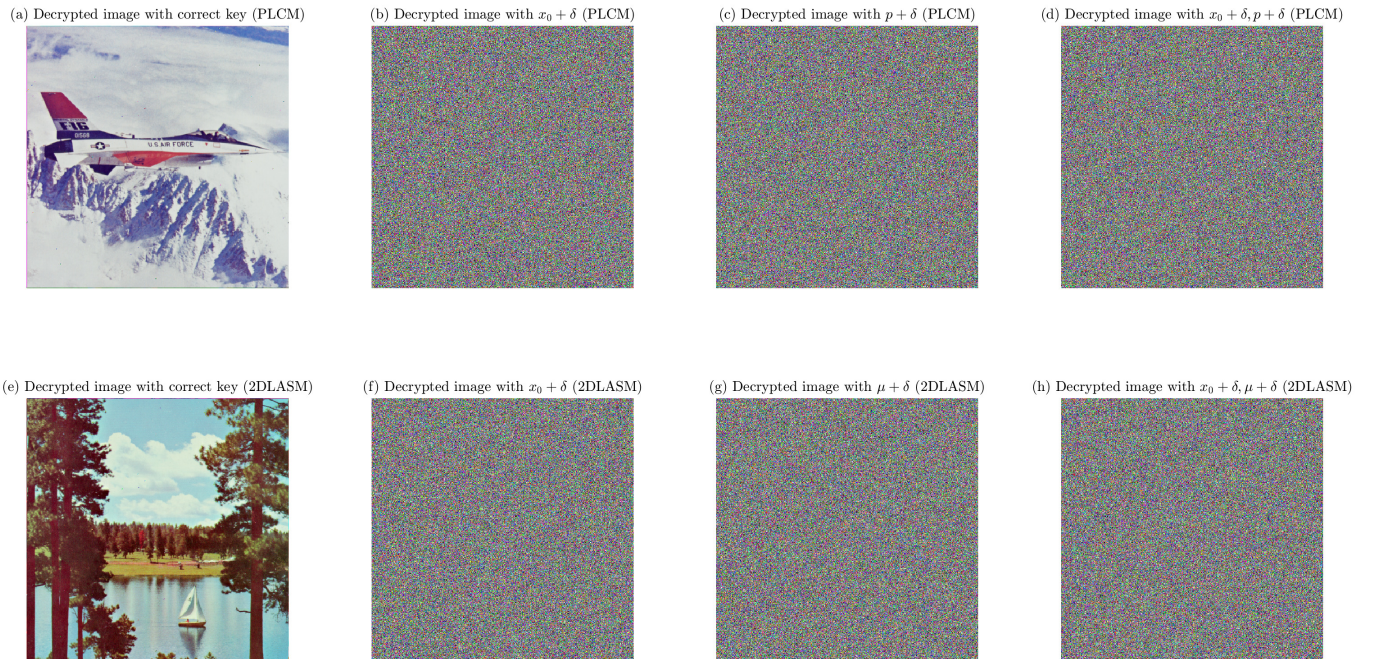
Figure 5: Key sensitivity analysis. (a) decrypt image using PLCM with correct key, (b) decrypt image using PLCM with $x_0 + \delta$, (c) decrypt image using PLCM with $p + \delta$, (d) decrypt image using PLCM with $x_0 + \delta$ and $p + \delta$, (e) decrypt image using 2DLASM with correct key, (f) decrypt image using 2DLASM with $x_0 + \delta$, (g) decrypt image using 2DLASM with $\mu + \delta$, (h) decrypt image using 2DLASM with $x_0 + \delta$ and $p + \delta$. The increment δ is set to 1×10^{-9}.

5.2. Resistance To Differential Attacks

To resist differential attacks, the encryption algorithms should have high sensitivity to the plain image, that is, a minor change in the plain image will lead to a completely change in the cipher image [41]. To evaluate the ability of the proposed strategy to resist such attacks, Number of Pixels Change Rate (NPCR) and Unified Average Changing Intensity (UACI) are calculated [42]. NPCR can be calculated according to the following equation:

$$\text{NPCR} = \sum_{i=0}^{w} \sum_{j=0}^{h} \frac{D(i, j)}{w \times h} \times 100\%, \quad (15)$$

where w and h denote the width and the height of the images, $D(i, j)$ is defined as follows:

$$D(i, j) = \begin{cases} 1, & F_c^1[i, j] \neq F_c^2[i, j], \\ 0, & F_c^1[i, j] = F_c^2[i, j], \end{cases} \quad (16)$$

F_c^1 and F_c^2 are two cipher images generated with the plain image and the slightly changed plain image, respectively, $F_c[i, j]$ is the pixel value. UACI is given by:

$$\text{UACI} = \sum_{i=0}^{w} \sum_{j=0}^{h} \frac{|F_c^1[i, j] - F_c^2[i, j]|}{w \times h \times 255} \times 100\%, \quad (17)$$

According to Refs. [43, 44], for an image of size 512×512, when the significance level is equal to 0.05, the expected values of NPCR and UACI are 99.5893% and [33.3730%, 33.5541%], respectively. An image encryption scheme passes the diffusion property test when NPCR is higher than the expected value, and UACI falls within the interval.

In the proposed strategy, despite all assistant threads perform diffusion operations independently, they take the last pixel of the next subframe as the diffusion seed to reconstruct the relationship between all subframes. This guarantees that one pixel changed in any subframe, will result in a completely different cipher frame. To fully evaluate the resistance of the proposed strategy to differential attacks, we generate byte sequences, encrypt a set of plain images, randomly select and change a pixel in the plain images, encrypt the modified images with the same byte sequences, calculate NPCR and UACI between the generated cipher images. For each plain image, we repeat above steps for 100 times, fetch the minimum, maximum, and average values, and list the results in Tab. 8.

Table 8: Results of NPCR and UACI

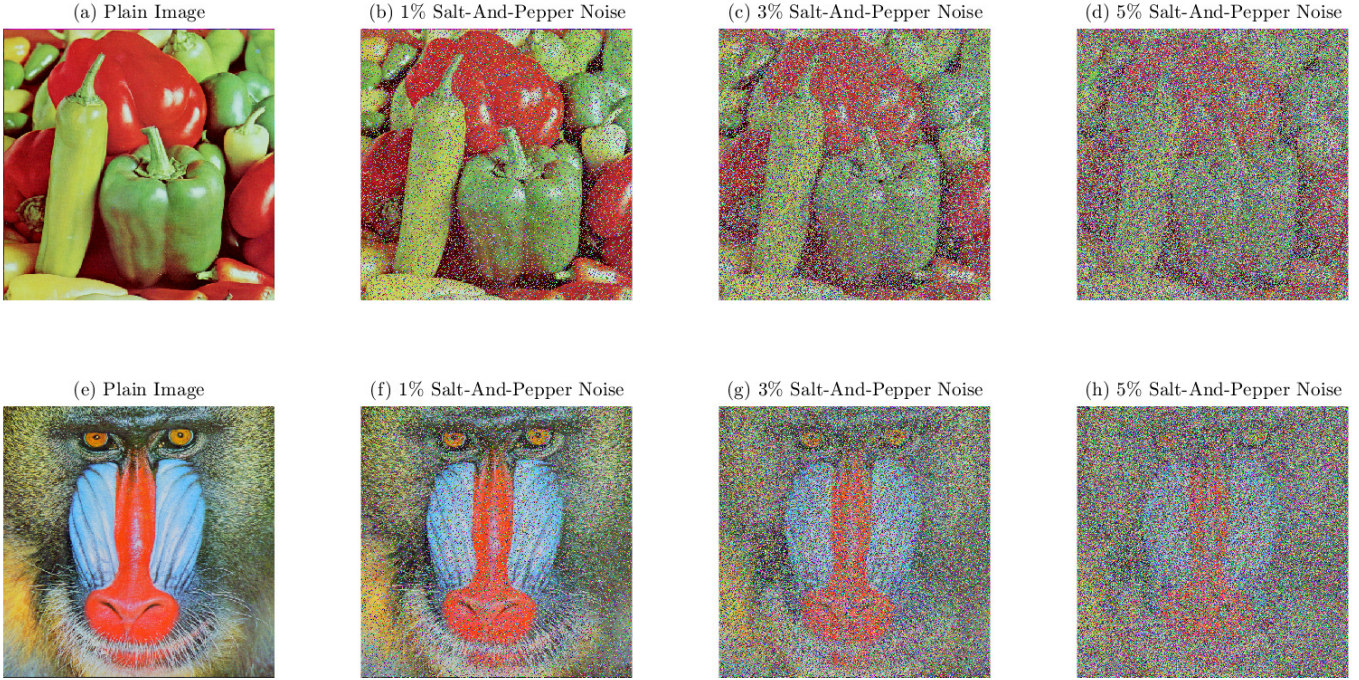| Test | Image | PRBG | Channel | | | | | | | | |
| | | | R | | | G | | | B | | |
			Min	Max	Average	Min	Max	Average	Min	Max	Average
NPCR	Lena	CPLCM	99.5770	99.6334	99.6093	99.5762	99.6361	99.6096	99.5781	99.6372	99.6048
		2DLASM	98.9208	99.6376	99.5696	99.1913	99.6395	99.5667	99.2020	99.6414	99.5839
	Airplane	CPLCM	99.5800	99.6471	99.6092	99.5789	99.6426	99.6093	99.5861	99.6418	99.6091
		2DLASM	98.4215	99.6349	99.5496	98.4520	99.6433	99.5409	98.4180	99.6403	99.5138
	Lake	CPLCM	98.5302	99.6841	99.5808	96.8250	99.6315	99.5587	98.4116	99.6395	99.5757
		2DLASM	98.6176	99.6284	99.5616	99.1982	99.6384	99.5949	99.1920	99.6445	99.5709
	Peppers	CPLCM	98.4627	99.6361	99.5762	98.4226	99.6510	99.5301	99.2138	99.6407	99.5908
		2DLASM	97.2801	99.6559	99.5536	97.3145	99.6437	99.5582	98.6259	99.6391	99.5693
	Mandrill	CPLCM	97.2404	99.6464	99.5532	98.8369	99.6407	99.5809	98.4257	99.6304	99.5529
		2DLASM	98.4825	99.7314	99.5763	98.7518	99.6433	99.5658	98.6263	99.6418	99.5753
	Splash	CPLCM	98.6454	99.6368	99.5792	98.4016	99.6349	99.5604	98.8396	99.6330	99.5838
		2DLASM	98.4062	99.6349	99.5779	98.4413	99.6376	99.5171	98.4142	99.6357	99.5463
UACI	Lena	CPLCM	33.3000	33.5896	33.4585	33.3756	33.6102	33.4633	33.3486	33.5817	33.4616
		2DLASM	33.3106	33.6019	33.4648	33.3245	33.5847	33.4678	33.3580	33.5815	33.4674
	Airplane	CPLCM	33.3524	33.5590	33.4615	33.3716	33.5565	33.4650	33.3379	33.5907	33.4682
		2DLASM	33.3349	33.5936	33.4680	33.3895	33.6084	33.4678	33.3561	33.5746	33.4734
	Lake	CPLCM	33.3271	33.5673	33.4630	33.3637	33.5900	33.4675	33.3601	33.5879	33.4668
		2DLASM	33.3629	33.5763	33.4700	33.3610	33.5877	33.4558	33.3493	33.5729	33.4652
	Peppers	CPLCM	33.3690	33.5836	33.4623	33.3517	33.5588	33.4577	33.3644	33.5995	33.4632
		2DLASM	33.3299	33.5721	33.4585	33.3322	33.5540	33.4664	33.3713	33.5711	33.4687
	Mandrill	CPLCM	33.3343	33.5772	33.4643	33.3393	33.5597	33.4644	33.3561	33.5829	33.4603
		2DLASM	33.3706	33.5938	33.4720	33.3503	33.5429	33.4555	33.3110	33.6242	33.4626
	Splash	CPLCM	33.3785	33.5953	33.4662	33.3411	33.5438	33.4536	33.3535	33.5860	33.4630
		2DLASM	33.3427	33.5976	33.4647	33.3602	33.6073	33.4600	33.3805	33.5635	33.4619

Figure 6: Resistance to noise. (a) plain image peppers, (b)-(d) decrypt the cipher image with 1%, 3%, 5% salt-and-pepper noise using PLCM, (e) plain image mandrill, (f)-(h) decrypt the cipher image with 1%, 3%, 5% salt-and-pepper noise using 2DLASM,.
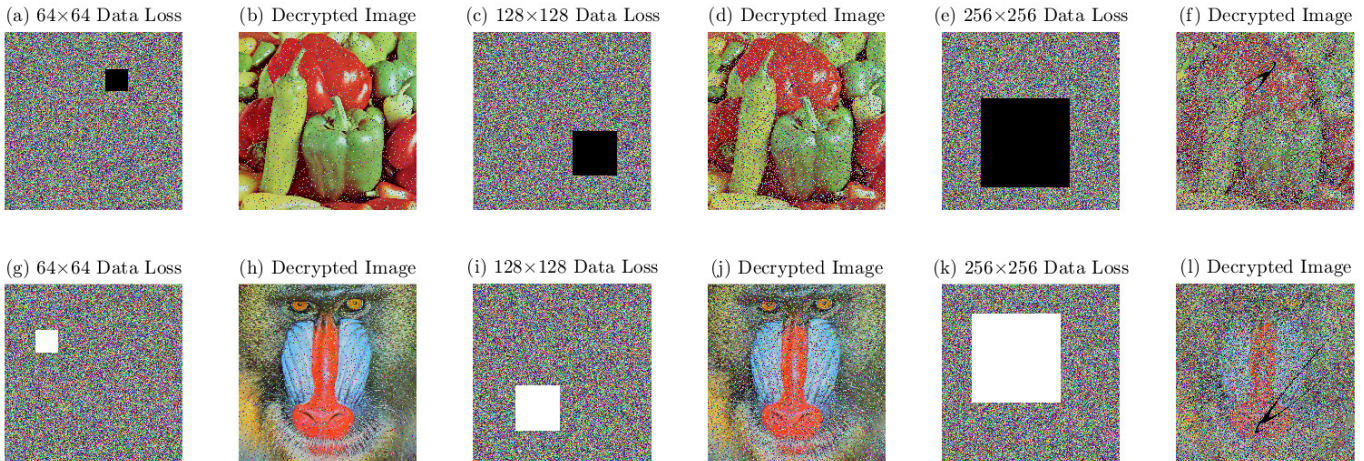

Figure 7: Resistance to data loss. (a)-(f) cipher images with different data losses and the corresponding images decrypted with PLCM, (g)-(j) cipher images with different data losses and the corresponding images decrypted with 2DLASM.

5.3. Resistance To Noise And Data Loss

Images or video frames may be affected by noise while transmitting over the channel. When a cipher image has noise or losses part of data, the cyrptosystem needs to recover the original image with high visual quality [45]. To evaluate the robustness, we use the two deployed cryptosystems to encrypt a plain image with randomly selected keys, add 1%, 3%, and 5% salt-and-pepper noise [46] to the generated cipher images, use the same keys to decrypt the cipher images, and plot the plain and decrypted images in Fig. 6. Although the decrypted image are changed when there exists noise in the cipher image, the approximate information of the plain image is preserved, even when the slat-and-pepper noise as high as 5%.

In real application, image cropping is very common, which may lead to data loss [47]. To assess the capability of the proposed strategy to resist the data loss, similarly, we use the deployed cryptosystems to encrypt a plain image, randomly select and remove 64×64, 128×128, or 512×512 blocks from the cipher images, replace the removed block with white or black blocks, decrypt the modified cipher images with the same keys, and show the results in Fig. 7. Clearly, the contours of the plain images are preserved, even though 256×256 blocks are removed from the cipher images. That is, when there exist 25% data loss in the cipher image, the deployed cryptosystems can still recover the information of the plain image. The proposed strategy, therefore, can resist noise and data loss.
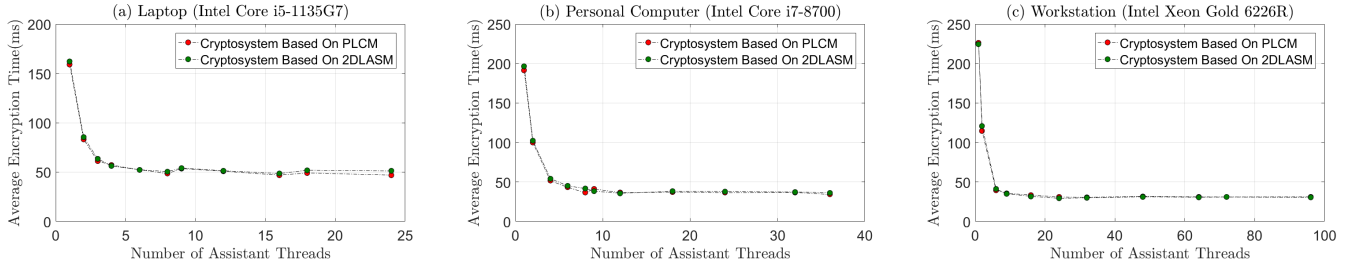
11

Figure 8: Relationship between the number of assistant threads and the encryption speed, (a) results of the laptop (Intel Core i5-1135G7), (b) results of the personal computer (Intel Core i7-8700G7), (c) results of the workstation (Intel Xeon Gold 6226R).
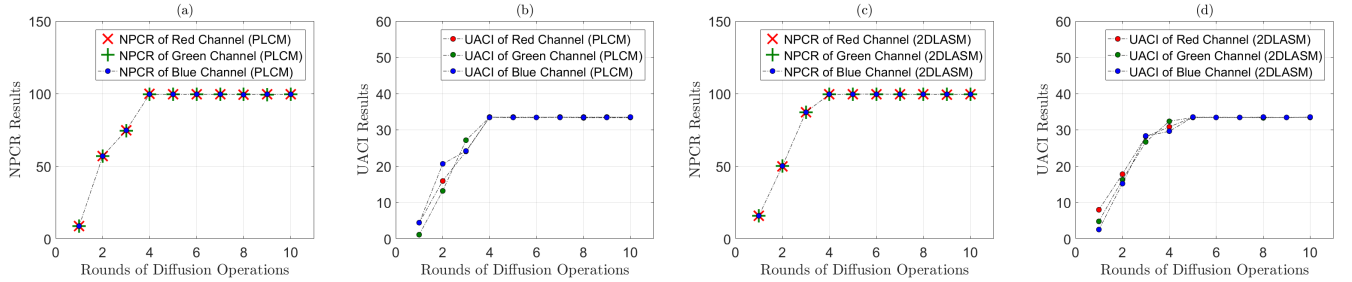

Figure 9: Relationship between the rounds of diffusion operations and NPCR, UACI results, (a) NPCR results of the cryptosystem based on PLCM, (b) UACI results of the cyrp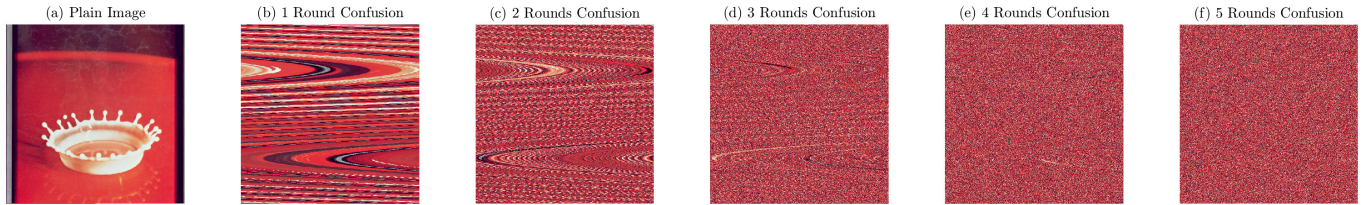tosystem based on PLCM, (c) NPCR results of the cryptosystem based on 2DLASM, (d) UACI results of the cyrptosystem based on 2DLASM.

Figure 10: Results of confusion operations. (a) plain image splash, (b)-(f) images after different rounds of confusion operations, .

6. Parameter Setup

According to the encryption process, clearly, the number of assistant threads n and the rounds of confusion and diffusion r significantly affect the the encryption speed and the statistical performance of the deployed cryptosystems. In all experiments carried out in this paper, n is set to 8, 12, and 32 for laptop, personal computer, and workstation, respectively, and r is set to 5. The reasons for such settings are analyzed in this section.
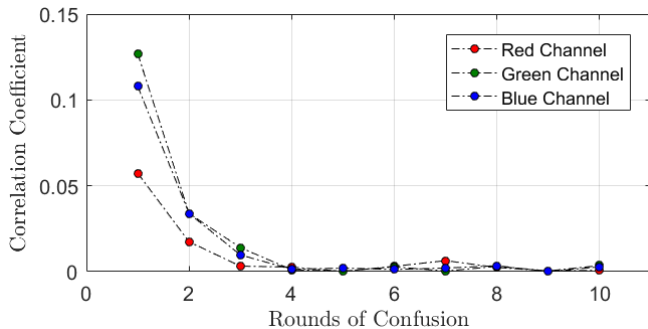

Figure 11: Correlation coefficient between the plain image and the images after different rounds of confusion operations.

We use different number of assistant threads to encrypt a plain video of size 576×576 using three hardware platforms. The relationship between the average encryption time and the number of assistant threads are drawn in Fig. 8. Set n to the maximum number of threads supported by CPU is unnecessary, however, can guarantee the deployed cryptosystems reach their fastest encryption speed.

The purposes of diffusion and confusion operations are to improve the plaintext sensitivity of the cryptosystems and decrease the correlation of the plain images. We, thus, generate byte sequences, perform 10 rounds of diffusion operations on a plain image, randomly select a pixel, change its value, perform 10 rounds of diffusion operations on the modified image with the same byte sequences, and calculate NPRC and UACI between the generated cipher images. The results are plotted in Fig. 9. Similarly, we perform 10 rounds of confusion operations on a plain image. The plain image and the scrambled images after 1-5 rounds of confusion operations are shown in Fig. 10. The correlation coefficients between the plain image and the scrambled images after different rounds of confusion operations are drawn in Fig. 11. When r is equal to 5, clearly, NPCR, UACI, and the correlation coefficient reach the upper and lower bounds, respectively.

12

7. Comparison To Previous Works

As discussed above, existing algorithms can be divided into full and selective video encryption. The proposed strategy, clearly, belongs to the former category. In this section, therefore, the deployed cryptosystems are compared with several recent published papers on full video encryption. The results are shown in Tab. 9. For some selected works, videos of different sizes are used to evaluate the encryption speed. We list the encryption speed for the largest videos in the table.

With the development of information science and hardware, the users put forward higher requirements for security. Thus almost all the latest works are based on confusion-diffusion architecture. To the best of our knowledge, however, these works only consist of one round of confusion and diffusion operation to improve the computational efficiency. And they cannot meet the requirements of real-time encryption, that is, the average encryption time (ms) of video frames is less than 1000 / FPS. Therefore, compare to previous works, the proposed strategy achieves the following advantages:

i) It realizes real-time video encryption, provides a feasible solution for related applications, and points out a new path for related research.

ii) By taking advantages of parallel computing technique, it proves that real-time video encryption based on multi-round confusion-diffusion architecture is possible, and thus improves the security of real-time video encryption to the level of image encryption.

iii) It works with many confusion, diffusion methods, and different chaotic maps.

iv) It can be easily implemented with both software and hardware such as ARM, FPGA, etc.

8. Conclusion

To sum up, a parallel computing technique based real-time chaotic video encryption strategy is proposed in this paper. It uses multiple threads to simultaneously perform confusion and diffusion operations on corresponding subframes to improve the computational efficiency. To evaluate the performance of the strategy, two chaotic maps are selected to implement cryptosystems. The encryption speed evaluation prove that such strategy significantly improves the encryption speed, and realizes real-time video encryption with different hardware platforms. The statistical and security analysis show that the deployed cryptosystems have outstanding statistical properties and resistance to attacks, noise, and data loss. Compared with previous works, the proposed strategy, to the best of our knowledge, achieves the fastest encryption speed, realizes the first real-time video encryption based on multiple-round confusion-diffusion architecture. This paper provides a feasible solution and a new path for related applications and research, respectively.

CRediT authorship contribution statement

Dong Jiang: Conceptualization, Methodology, Writing-original draft, Software, Supervision. **Zhen Yuan:** Investigation, Methodology, Software . **Wen-xin Li**: Investigation, Software. **Liang-liang Lu:** Conceptualization, Methodology, Writing - review & editing, Supervision.

Declaration of competing interest

The authors declare that they have no known competing financial interests or personal relationships that could have appeared to influence the work reported in this paper.

Table 9: Speed comparison to previous works

Algorithm	r_c	r_d	CPU	Memory	Video Size	CS	AET(ms)	RTE
Ref. [17]	1	1	Pentium 4@3.2GHz	4GB	240×360	RGB	1059 (8D Map) 2314 (12D Map) 1357 (Ikeda DDE)	$\times$ $\times$ $\times$
Ref. [18]	1	1	–	–	240×360	RGB	472	$\times$
Ref. [19]	1	1	Intel Core i3-2130@3.4GHz	4GB	352×288	YUV	5960†	$\times$
Ref. [20]	1	1	Intel Core i5-2400@3.1GHz	4GB	–	RGB	408	$\times$
Ref. [21]	1	1	Intel Core i7-8750H@2.2GHz	16GB	352×288	RGB	260	$\times$
Ref. [22]	1	1	Intel Core i5-6200U@2.3GHz	8GB	360×240	RGB	5497	$\times$
Ours	5	5	Intel Core i5-1135G7@2.4GHz	8GB	480×480	RGB	36.26 (PLCM) 35.49 (2DLASM)	$\checkmark$ $\checkmark$
			Intel Core i7-8700@3.2GHz	32GB	576×576	RGB	39.92 (PLCM) 40.67 (2DLASM)	$\checkmark$ $\checkmark$
			Intel Xeon Gold 6226R@2.9GHz	64GB	768×768	RGB	36.56 (PLCM) 36.23 (2DLASM)	$\checkmark$ $\checkmark$

r_c: rounds of confusion; r_d: rounds of diffusion; CS: Color Space; AET: Average Encryption Time; RTE: Real-Time Encryption (AET $\leq$ 1000 / FPS); –: not specified; $\dagger$: the accurate average encryption time is not described in Ref. [19], but is given in Ref. [21].

Data availability

Data will be made available on request.

Acknowledgments

References

[1] Pareek NK, Patidar V, Sud KK. Image encryption using chaotic logistic map. Image Vision Comput 2006; 24:926-934.

[2] Fang P, Liu H, Wu C, Liu M. A survey of image encryption algorithms based on chaotic systesm. Visual Comput 2022; 2022: 1-29.

[3] Zhang Y, Wang B. Optical encryption based on interference. Opt Lett 2008; 33: 2443-2445.

[4] Zhang Y, Wang X. A symmetric image encryption algorithm based on mixed linear–nonlinear coupled map lattice. Inform Sciences 2014; 273: 329-351.

[5] Tedmori S, AI-Najdawi N. Image cryptographic algorithm based on the Haar wavelet transform. Inform Sci 2014; 269: 21-34.

[6] Chai x, Gan Z, Chen Y, Zhang Y. A visually secure image encryption scheme based on compressive sensing. Signal Process 2017; 134:35-51.

[7] Luo Y, Zhou R, Liu J, Cao Y, Ding X. A parallel image encryption algorithm based on the piecewise linear chaotic map and hyper-chaotic map. Nonlinear Dynam 2018; 93:1165-1181.

[8] Zia U, McCartney M, Scotney B, Martinez J, AbuTair M, Memon J. Survey on image encryption techniques using chaotic maps in spatial, transform and spatiotemporal domains. Int J Inf Secur 2022; 21:917-935.

[9] Chen J, Zhu Z, Fu C, Yu H. A fast image encryption scheme with a novel pixel swapping-based confusion approach. Nonlinear Dynam 2014; 77:1191-1207.

[10] Wong K, Kwok B, Yuen C. An efficient diffusion approach for chaos-based image encryption. Chaos Soliton Fract 2009; 41:2652-2663.

[11] Matthews R. On the derivation of a "chaotic" encryption algorithm. Cryptologia 1989; 13:29-42.

[12] Massoudi A, Lefebvre F, De Vleeschouwer C, Macq B, Quisquater JJ. Overview on selective encryption of image and video: challenges and perspectives. Eurasip J Inf Secur 2008; 2008:179290.

[13] Liu F, Koenig H. A survey of video encryption algorithms. Comput Secur 2010; 29: 3-15.

[14] Chiaraluce F, Ciccarelli L, Gambi E, Pierleoni P, Reginelli M. A new chaotic algorithm for video encryption. IEEE T Consum Electr 2002; 48:838-844.

[15] Lian S, Sun J, Wang J, Wang Z. A chaotic stream cipher and the usage in video protection. Chaos Soliton Fract 2007; 34:851-859.

[16] Yang S, Sun S. A video encryption method based on chaotic maps in DCT domain. Prog Nat Sci 2008; 18:1299-1304.

[17] Valli D, Ganesan K. Chaos based video encryption using maps and Ikeda time delay system. Eur Phys J Plus 2017; 132:1-18.

[18] Kumar RR, Ganeshkumar D, Suresh A, Manigandan K. A new one round video encryption scheme based on 1D chaotic maps. in: 2019 5th Int Conf Adv Comput Commun Syst; 2019:439-444.

[19] Li x, Yu H, Zhang H, Jin X, Sun H, Liu J. Video encryption based on hyperchaotic system. Multimed Tools Appl 2020; 79:23995-24011.

[20] Yasser I, Mohamed A, Samra AS, Khalifa F. A chaotic-based encryption/decryption framework for secure multimedia communications. Entropy 2020; 22:1253.

[21] Hosny KM, Zaki MA, Lashin NA, Hamza HM. Fast colored video encryption using block scrambling and multi-key generation. Visual Comput 2022; 2022:1-32.

[22] Dua M, Makhija D, Manasa PYL, Mishra P. 3D chaotic map-cosine transformation based approach to video encryption and decryption. Open Comput Sci 2022; 12:37-56.

[23] Hamidouche W, Farajallah M, Sidaty N, Assad S, Deforges O. Real-time selective video encryption based on the chaos system in scalable HEVC extension. Signal Process: Image Commun 2017; 58:73-86.

[24] Chen H, Tanougast C, liu Z, Blondel W, Hao B. Optical hyperspectral image encryption based on improved Chirikov mapping and gyrator transform. Opt Laser Eng 2018; 107:62-70.

[25] Fu C, Chen J, Zou H, Meng W, Zhan Y, Yu Y. A chaos-based digital image encryption scheme with an improved diffusion strategy. Opt Express 2012; 20:2363-2378.

[26] Zhong J, Jiang D, Huang Q, Cao Y. A self-updating digital chaotic stream cipher. Int J Mod Phys 2018; 29:1850074.

[27] Hua Z, Zhou Y. Image encryption using 2D Logistic-adjusted-Sine map. Inform Sci 2016; 339:237-253.

[28] Li c, Lin D, Feng B, Lv J, Hao F. Cryptanalysis of a chaotic image encryption algorithm based on information entropy. IEEE Access 2018; 6: 75834-75842.

[29] Man Z, Li J, Di X, Sheng Y, Liu Z. Double image encryption algorithm based on neural network and chaos. Chaos Soliton Fract 2021; 152:111318.

[30] Kwok HS, Tang WKS. A fast image encryption system based on chaotic maps with finite precision representation. Chaos Soliton Fract 2007; 32:1518-1529.

[31] Zhang X, Zhao Z, Wang J. Chaotic image encryption based on circular substitution box and key stream buffer. Singal Process 2014; 29:902-913.

[32] Ye G, Wong KW. An efficient chaotic image encryption algorithm based on a generalized Arnold map. Nonlinear Dynam 2012; 69:2079-2087.

[33] Rhouma R, Meherzi S, Belghith S. OCML-based colour image encryption. Chaos Soliton Fract 2009; 40:309-318.

[34] Belazi A, Khan M, El-Latif AAA, Belghith S. Efficient cryptosystem approaches: S-boxes and permutation-substitution-based encryption. Nonlinear Dynam 2018; 87:337-361.

[35] Wu Y, Zhou Y, Saveriades G, Agaian S, Noonan JP, Natarajan P. Local Shannon entropy measure with statistical tests for image randomness. Inform Sci 2013; 222:323-342.

[36] Artiles JAP, Chaves DPB, Pimentel C. Image encryption using block cipher and chaotic sequences. Signal Process 2019; 79:24-31.

[37] Xian Y, Wang X. Fractal sorting matrix and its application on chaotic image encryption. Infrom Sci 2021; 547:1154-1169.

[38] Rukhin A,et al. A statistical test suite for random and pseudorandom number generators for cryptographic applications. NIST Special Publication 800-22, Revision 1.a 2010.

[39] Wang X, Teng L, Qin X. A novel colour image encryption algorithm based on chaos. Signal Process 2012; 92:1101-1108.

[40] Alvarez G, Li S. Some basic cryptographic requirements for chaos-based cryptosystems. Int J Bifurcat Chaos 2006; 16:2129-2151.

[41] Khan M, Massod F. A novel chaotic image encryption technique based on multiple discrete dynamical maps. Multimed Tools Appl 2019; 78:26203-26222.

[42] Luo Y, Yu J, Lai W, Liu L. A novel chaotic image encryption algorithm based on improved baker map and logistic map. Multimed Tools Appl 2019; 78: 22023-22043.

[43] Mansouri A, Wang X. A novel one-dimensional sine powered chaotic map and its application in a new image encryption scheme. Inform Sci 2020; 520:46-62.

[44] Talhaoui MZ, Wang X. A new fractional one dimensional chaotic map and its application in high-speed image encryption. Infrom Sci 2021; 550:13-26.

[45] Chen H, Bai E, Jiang X, Wu Y. A Fast Image Encryption Algorithm Based on Improved 6-D Hyper-Chaotic System. IEEE Access 2022; 10:116031-116044.

[46] Azzeh J, Zahran B, Alqadi Z. Salt and pepper noise: Effects and removal. JOIV: Int J Inform Visual 2018; 2:252-256.

[47] Gan Z, Chai X, Han D, Chen Y. A chaotic image encryption algorithm based on 3-D bit-plane permutation. Neural Comput Appl 2019; 31:7111-7130.